Research Article

Wenqian Gong, Yiyu Shi, Zhenxing Liu, Chi Zhang, Zhiwei Cui*, Yu Chen and Xinxing Zhou*

# Breakdown of the effective medium theory: a perspective from Goos–Hänchen shift

https://doi.org/10.1515/nanoph-2025-0314
Received July 9, 2025; accepted August 26, 2025;
published online September 5, 2025

**Abstract:** The effective medium theory (EMT) provides a simplified framework to calculate the electromagnetic responses and is generally considered exact in the all-dielectric system with deep-subwavelength constituents. In this work, we perform the Goos–Hänchen (GH) shift that invalidates the EMT on the multilayered dielectric structures under the common conditions. This breakdown of the EMT arises from the high sensitivity of the GH shift on the phase and magnitude of Fresnel reflection coefficient. The degree of such breakdown shows strong dependence on the polarization angle of incidence and the layer and filling fraction of the structures. Notably, we find that the GH shift is potentially applicable to nano-meter scale thickness sensing, which cannot be displayed based on EMT in some cases. Our findings will provide useful guidance to reduce the calculation errors of the electromagnetic responses and promote the design of precise metrology devices.

**Keywords:** effective medium theory; Goos–Hänchen shift; breakdown; nanoscale sensing

## 1 Introduction

The calculation of the electromagnetic responses in the subwavelength-sized inhomogeneous structures is complex and difficult. To solve this problem, the effective medium theory (EMT) is proposed [1], [2]. Its conceptual process involves replacing the inhomogeneous structures with a homogeneous "effective medium" with uniform properties. This provides the fundamental approximation method to obtain the same response as the complex inhomogeneous structures to the identical excitation. In practice, its two predominant frameworks are the Maxwell–Garnett EMT [3] and Bruggeman EMT [4]. The former is applied in reliable predictions for electro-magnetic properties in a continuous host medium containing sparse inclusions at low volume fractions. In contrast, the latter enables precise modeling of the dielectric permittivity and conductivity of the high-concentration systems near the percolation threshold. To date, the EMT has been widely used in the description of the index of permittivity [5]–[7], permeability [8], [9], and surface conductivity [10]–[12] of complex materials, to name a few. Importantly, the effective medium can exhibit the extraordinary characteristics such as birefringence [13], Anderson localization [14], negative refractive index [15]–[17], and near-zero permittivity [18], [19], and leads to the significant findings like the metasurface [20]–[22], cloak [23], [24], and super-lens [25]–[27].

Despite its extensive applications, the EMT will be invalid in some cases. Typically, the EMT fails to describe the homogenization of the periodic metal-dielectric structures involving the large wave vectors, especially when the metal plasmons and hyperbolic high-$k$ modes exist [28]–[30]. The underlying mechanism behind this phenomenon is ascribed to the inappropriate homogenization of the local structure properties that can strongly influence the overall structure properties. Therefore, the all-dielectric systems that do not support the large wave vectors are believed to be adaptable to the EMT for a long time. In recent years, it has

Wenqian Gong and Yiyu Shi contributed equally to this work.

***Corresponding authors: Zhiwei Cui**, School of Physics, Xidian University, Xi'an, 710071, China, E-mail: zwcui@mail.xidian.edu.cn.
https://orcid.org/0000-0001-8338-4270; and **Xinxing Zhou**, Key Laboratory of Low-Dimensional Quantum Structures and Quantum Control of Ministry of Education, School of Physics and Electronics, Hunan Normal University, Changsha 410081, China; Key Laboratory of Physics and Devices in Post-Moore Era, College of Hunan Province, Changsha 410081, China; and Hunan Research Center of the Basic Discipline for Quantum Effects and Quantum Technologies, Hunan Normal University, Changsha 410081, China, E-mail: xinxingzhou@hunnu.edu.cn.
https://orcid.org/0000-0002-8678-906X
**Wenqian Gong**, **Zhenxing Liu and Chi Zhang**, Key Laboratory of Low-Dimensional Quantum Structures and Quantum Control of Ministry of Education, School of Physics and Electronics, Hunan Normal University, Changsha 410081, China
**Yiyu Shi**, School of Physics, Xidian University, Xi'an, 710071, China
**Yu Chen**, International Collaborative Laboratory of 2D Materials for Optoelectronics Science and Technology, Institute of Microscale Optoelectronics, Shenzhen University, Shenzhen 518060, China,
E-mail: yuchen@szu.edu.cn. https://orcid.org/0000-0001-9926-2518

been found that the EMT will also be invalid in the all-dielectric systems [31]–[35]. Sheinfux et al. first theoretically proposed the breakdown of EMT in a purely dielectric structure near the critical angle [31], which was later experimentally verified by Zhukovsky et al. [32]. Furthermore, the similar phenomena for the evanescent waves are successively predicted and observed in the one-dimensional disordered deep-subwavelength optical system due to the Anderson localization [33], [34]. Lately, a fundamental breakdown of the EMT by the photonic spin Hall effect in all-dielectric systems has been reported [35]. It stems from the spin–orbit interaction of light that is sensitive to the slight phase accumulations during the wave propagation. These works reveal that, not only the magnitude, but also the phase deviation of Fresnel reflection coefficients calculated by EMT may have great impacts on the final electromagnetic response. The Goos–Hänchen (GH) shift is the longitudinal beam shift in the incident plane [36], and attracted intensive attention due to its potential applications in precise sensing [37]–[39]. Besides, it is usually studied in the framework of EMT [40]–[42]. Now, an interesting question arises: as the typical electromagnetic response associated with the Fresnel reflection coefficient phase and magnitude, will the GH shift invalidate the EMT in the general all-dielectric system?

To address this question, we calculate the spatial and angular GH shifts on the all-dielectric periodic multilayered structures via the EMT and transfer matrix method (TMM), respectively, in this work. Numerical results show that the breakdown of EMT will emerge under the general conditions even without the critical angle. The physical mechanism is that the GH shift is very sensitive to the phase and magnitude of the Fresnel reflection coefficient. Besides, we examine the effects of the polarization angle of the incidence and the layer and filling fraction of the structures on the degree of EMT breakdown. Finally, we reveal the potential application of the GH shift on the detection of structure defects at the extreme nanoscale, which cannot be demonstrated in the EMT framework in some cases. These results can deepen the understanding of the EMT in various application realms and further the design of the relevant devices.

## 2 Theoretical model and numerical method

We will illustrate our idea by considering an all-dielectric periodic multilayered structure composed of $N$ pairs of $TiO_2$ and $Al_2O_3$ with permittivities $\varepsilon_1$ and $\varepsilon_2$, and thicknesses $d_1$ and $d_2$, respectively, and the superstrate ZnSe and substrate $Si_3N_4$ with permittivities $\varepsilon_{\text{inc}}$ and $\varepsilon_{\text{out}}$, as shown in Figure 1(a). The Fresnel reflection and refraction coefficients of such a structure can be rigorously calculated by the TMM as [43]

$$\begin{bmatrix} t \\ 0 \end{bmatrix} = M_{\text{out},2} P_2 \left(M_{2,1} P_1 M_{1,2} P_2\right)^{N-1} M_{2,1} P_1 M_{1,\text{inc}} \begin{bmatrix} 1 \\ r \end{bmatrix} = Q^{\text{TMM}} \begin{bmatrix} 1 \\ r \end{bmatrix}, \tag{1}$$

with the converting $M$ and propagating $P$ matrix expressed as

$$M_{i,j} = \frac{1}{2}\begin{bmatrix} 1+\Delta_{i,j} & 1-\Delta_{i,j} \\ 1-\Delta_{i,j} & 1+\Delta_{i,j} \end{bmatrix}, \quad P_i = \begin{bmatrix} e^{ik_{iz}d_i} & 0 \\ 0 & e^{-ik_{iz}d_i} \end{bmatrix}, \tag{2}$$

where $k_{iz} = k_0\sqrt{\varepsilon_i - \varepsilon_{\text{in}}\sin^2\theta_i}$, $\Delta_{i,j} = k_{jz}/k_{iz}$ and $\Delta_{i,j} = \varepsilon_j k_{iz}/(\varepsilon_i k_{jz})$ for $s$- and $p$-polarized incidence, respectively, subscript $i$ and $j$ stand for the $i$-th and $j$-th layer, $k_0$ is the wave number in vacuum, and $\theta_i$ is the incident angle. Finally, the $r^{\text{TMM}}$ and $t^{\text{TMM}}$ can be written as

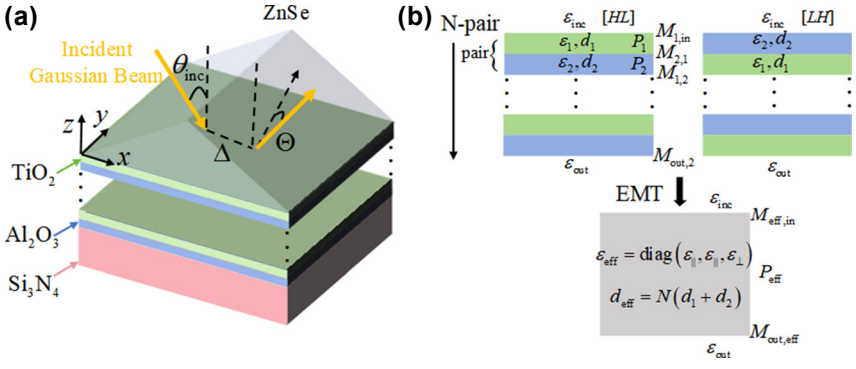


**Figure 1:** Illustrations of the GH shifts and the EMT. (a) Schematic of an all-dielectric periodic multilayered structure containing low-index ($L$) layers made of alumina ($Al_2O_3$), high-index ($H$) layers made of titania ($TiO_2$), a superstrate made of zinc selenide (ZnSe), and a substrate made of silicon nitride ($Si_3N_4$), and the spatial $\Delta$ and angular $\Theta$ GH shifts of the Gaussian beam with the incident angle $\theta_i$. (b) Schematic of the rigorous transfer matrix method (TMM) with the different stacking orderings [$LH$] and [$HL$], and effective medium theory (EMT).

$$r^{\mathrm{TMM}} = -\frac{Q_{21}^{\mathrm{TMM}}}{Q_{22}^{\mathrm{TMM}}}, \quad t^{\mathrm{TMM}} = Q_{11}^{\mathrm{TMM}} - \frac{Q_{12}^{\mathrm{TMM}} Q_{21}^{\mathrm{TMM}}}{Q_{22}^{\mathrm{TMM}}}. \tag{3}$$

For the EMT illustrated in Figure 1(b), such structure can be described as an effective uniaxial slab with relative permittivity $\overline{\overline{\varepsilon}} = \mathrm{diag}(\varepsilon_{\parallel}, \varepsilon_{\parallel}, \varepsilon_{\perp})$ with [1], [2]

$$\varepsilon_{\parallel} = \frac{\varepsilon_1 d_1 + \varepsilon_2 d_2}{d_1 + d_2}, \quad \varepsilon_{\perp} = \frac{\varepsilon_1 \varepsilon_2 (d_1 + d_2)}{\varepsilon_1 d_2 + \varepsilon_2 d_1}. \tag{4}$$

The Fresnel reflection and refraction coefficients between the superstrate and slab are

$$\begin{bmatrix} t \\ 0 \end{bmatrix} = M_{\mathrm{out,eff}} P_{\mathrm{eff}} M_{\mathrm{eff,inc}} \begin{bmatrix} 1 \\ r \end{bmatrix} = Q^{\mathrm{EMT}} \begin{bmatrix} 1 \\ r \end{bmatrix}, \tag{5}$$

where the matrices $M$ and $P$ have the similar forms as that in Eq. (2). $\Delta_{\mathrm{out,eff}} = k_{\mathrm{effz}}/k_{\mathrm{outz}}$ and $\Delta_{\mathrm{out,eff}} = \varepsilon_{\parallel} k_{\mathrm{outz}}/(\varepsilon_{\mathrm{out}} k_{\mathrm{effz}})$, $k_{\mathrm{effz}} = k_0 \sqrt{\varepsilon_{\parallel} - \varepsilon_{\mathrm{inc}} \sin^2 \theta_{\mathrm{inc}}}$ and $k_{\mathrm{effz}} = k_0 \sqrt{\varepsilon_{\perp} - \varepsilon_{\mathrm{inc}} \sin^2 \theta_{\mathrm{inc}}}$, and $\Delta_{\mathrm{eff,inc}} = k_{\mathrm{incz}}/k_{\mathrm{effz}}$ and $\Delta_{\mathrm{eff,inc}} = \varepsilon_{\mathrm{inc}} k_{\mathrm{effz}}/(\varepsilon_{\parallel} k_{\mathrm{incz}})$, for $s$- and $p$-polarized incidence, respectively. Meanwhile, the effective thickness $d_{\mathrm{eff}} = N(d_1 + d_2)$. Similarly, the $r^{\mathrm{EMT}}$ and $t^{\mathrm{EMT}}$ can be obtained as

$$r^{\mathrm{EMT}} = -\frac{Q_{21}^{\mathrm{EMT}}}{Q_{22}^{\mathrm{EMT}}}, \quad t^{\mathrm{EMT}} = Q_{11}^{\mathrm{EMT}} - \frac{Q_{12}^{\mathrm{EMT}} Q_{21}^{\mathrm{EMT}}}{Q_{22}^{\mathrm{EMT}}}. \tag{6}$$

Next, we proceed to derive the GH shift for reflection, i.e., the longitudinal centroid shift of the reflected beam. The vector angular spectrum of the incident Gaussian beam is [44]

$$\widetilde{\mathbf{E}}_i = \left[\cos\beta \hat{\mathbf{x}}_i + \sin\beta \hat{\mathbf{y}}_i - \frac{1}{k_0}(\cos\beta k_{ix} + \sin\beta k_{iy})\hat{\mathbf{z}}_i\right]\widetilde{u}_i, \tag{7}$$

with

$$\widetilde{u}_i(k_{ix}, k_{iy}) = \frac{w_0^2}{4\pi} e^{-\left(k_{ix}^2 + k_{iy}^2\right) w_0^2/4}, \tag{8}$$

where $\beta$ is the polarization angle, $w_0$ is the beam waist, and $k_{ix}$ and $k_{iy}$ are wave vector components along the $x_i$ and $y_i$ axes, respectively, in local coordinates $(x_i, y_i, z_i)$ for incidence. Based on the three-dimensional beam propagation model, the vector angular spectrum of the reflected Gaussian beam is expressed as

$$\begin{aligned} \widetilde{\mathbf{E}}_r = &\left[\cos\beta\left(r_p - \frac{\partial r_p}{\partial\theta_{\mathrm{inc}}}\frac{k_{rx}}{k_0}\right) + \sin\beta(r_p + r_s)\frac{k_{ry}}{k_0}\cot\theta_i\right] \\ &\times \widetilde{u}_r \hat{\mathbf{x}}_r + \left[\sin\beta\left(r_s - \frac{\partial r_s}{\partial\theta_{\mathrm{inc}}}\frac{k_{rx}}{k_0}\right)\right. \\ &\left. - \cos\beta(r_p + r_s)\frac{k_{ry}}{k_0}\cot\theta_i\right]\widetilde{u}_r \hat{\mathbf{y}}_r \\ &- \frac{1}{k_0}(\cos\beta r^p k_{rx} + \sin\beta r^s k_{ry})\widetilde{u}_r \hat{\mathbf{z}}_r, \end{aligned} \tag{9}$$

in which $k_{rx}$ and $k_{ry}$ are wave vector components in local coordinates $(x_i, y_i, z_i)$ for reflection and satisfying the relationships $k_{rx} = -k_{ix}$, $k_{ry} = k_{iy}$, and $\widetilde{u}_r(k_{rx}, k_{ry}) = \widetilde{u}_i(-k_{ix}, k_{iy})$.

The GH shift at any given plane $z = \mathrm{const}$ can be given by

$$\langle \mathbf{x} \rangle = \Delta + z\Theta = \frac{\left\langle \widetilde{\mathbf{E}}_r \middle| i\partial_{\mathbf{k}_{rx}} \middle| \widetilde{\mathbf{E}}_r \right\rangle}{\left\langle \widetilde{\mathbf{E}}_r | \widetilde{\mathbf{E}}_r \right\rangle} + \frac{z}{\sqrt{\varepsilon_{\mathrm{inc}}} k_0} \frac{\left\langle \widetilde{\mathbf{E}}_r \middle| \mathbf{k}_{rx} \middle| \widetilde{\mathbf{E}}_r \right\rangle}{\left\langle \widetilde{\mathbf{E}}_r | \widetilde{\mathbf{E}}_r \right\rangle}, \tag{10}$$

with $\partial_{\mathbf{k}_{rx}} = \hat{\mathbf{x}}_r \partial/\partial k_{rx}$ and $\mathbf{k}_{rx} = \hat{\mathbf{x}}_r k_{rx}$. Finally, the spatial ($\Delta$) and angular ($\Theta$) GH shifts in reflection of the arbitrary linearly polarized incident Gaussian beam can be derived as

$$\begin{aligned} \Delta &= \frac{1}{\sqrt{\varepsilon_{\mathrm{inc}}} k_0} \frac{\left|\cos\beta r_p\right|^2 \frac{\partial\phi_p}{\partial\theta_{\mathrm{inc}}} + \left|\sin\beta r_s\right|^2 \frac{\partial\phi_s}{\partial\theta_{\mathrm{inc}}}}{\left|\cos\beta r_p\right|^2 + \left|\sin\beta r_s\right|^2}, \\ \Theta &= -\frac{2}{\varepsilon_{\mathrm{inc}} k_0^2 w_0^2} \frac{|\cos\beta|^2 \frac{\partial |r_p|^2}{\partial\theta_{\mathrm{inc}}} + |\sin\beta|^2 \frac{\partial |r_s|^2}{\partial\theta_{\mathrm{inc}}}}{\left|\cos\beta r_p\right|^2 + \left|\sin\beta r_s\right|^2}, \end{aligned} \tag{11}$$

where $\beta$ is the polarization angle ($\beta = 0$ and $\beta = 90°$ denote the $p$- and $s$-polarization, respectively), and $\phi_{p,s}$ is the phase of $r_{p,s}$. Notably, the expression of the spatial ($\Delta$) GH shift derived by the stationary-phase analysis applies only when the reflection coefficient phase varies slowly.

## 3 Results and discussion

In the following numerical simulations, if no otherwise stated, we assume that the permittivities $\varepsilon_1$ and $\varepsilon_2$ of $TiO_2$ and $Al_2O_3$ are 6.67 [45] and 3.12 [46], respectively, the thicknesses $d_1$ and $d_2$ of $TiO_2$ and $Al_2O_3$ are 10 nm, permittivities $\varepsilon_{\mathrm{inc}}$ and $\varepsilon_{\mathrm{out}}$ of superstrate ZnSe and substrate $Si_3N_4$ are 6.65 [47] and 4.04 [48], respectively, the periodicity number of the structure $N_{\mathrm{pair}} = 10$, the stacking orderings of the multilayers is [$HL$], the polarization angle $\beta = 0$, the wavelength of incidence in vacuum is 0.6328 μm, and the beam waist of incidence is 27 μm. Besides, we emphasize that the results calculated by TMM are exact.

First, we check the invalidity of the EMT in the structure shown in Figure 1(a), via the performance of spatial and angular GH shifts. Under this scenario, the critical angle 51.23° exists at the interface between the superstrate and effective medium. Figure 2 illustrates breakdown of the EMT by the spatial and angular GH shifts on the all-dielectric

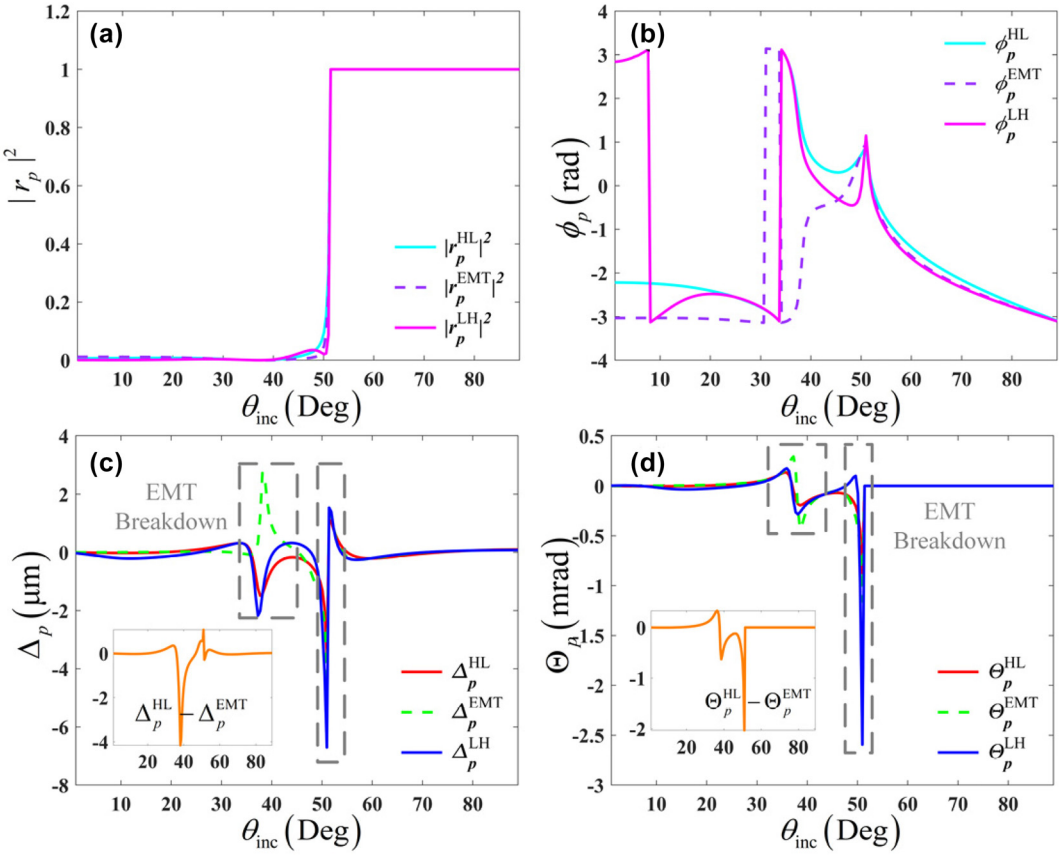


**Figure 2:** Breakdown of the EMT by the spatial (Δ) and angular (Θ) GH shifts on the all-dielectric periodic multilayered structures with different stacking orderings [*LH*] and [*HL*], in the case of $\varepsilon_{inc} = 6.65$. (a) Reflectivity $|r_p|^2$, (b) Fresnel reflection coefficient phase $\phi_p$, (c) spatial GH shifts (Δ), and (d) angular GH shifts (Θ).

periodic multilayered structures with different stacking orderings [*LH*] and [*HL*], in case of $\varepsilon_{inc} = 6.65$. According to the EMT, such a multilayered structure of both [*LH*] and [*HL*] will be homogenized to the same effective medium, which means the $\Delta_p^{EMT}(\Theta_p^{EMT})$ should be equal to the $\Delta_p^{HL}(\Theta_p^{HL})$ and $\Delta_p^{LH}$ $(\Theta_p^{LH})$. However, large discrepancies are found in these spatial and angular GH shifts. The discrepancies of angular GH shifts near the critical angle can be predicted according to the previous work [31], which are related to the deviations of reflectivity $|r_p|^2$. Notably, such discrepancies also appear far away from the critical angle (namely $\theta_i \in [35°, 45°]$), as highlighted by the gray squares. In this region, the EMT is valid from the perspective of reflectivity in general. Such a breakdown of EMT stems from the ultra-sensitivity of the angular GH shifts on the reflectivity. The similar discrepancies also emerge for the spatial GH shifts and are up to 4 μm at the $\theta_i \approx 40°$ far from the critical angle. It is ascribed to the deviation of Fresnel reflection coefficient phase $\phi_p$ which is closely related to the phase accumulation during the wave propagation. This process can occur in two ways: either the continuous way caused by the wave propagation in the medium, or the abrupt way induced by the wave reflection/transmission across the spatial boundary. The latter is sensitive to the stacking ordering, but the former is not. These phenomena indicate the strong dependence of the GH shift on the realistic stacking ordering of all-dielectric multilayers, even at the deep-subwavelength scale.

In terms of the previous works [31]–[34], the existence of a critical angle is a mandatory condition for the EMT breakdown in an all-dielectric system. Does it mean the GH shift calculated by the EMT is always exact in the all-dielectric structures without the critical angle? To tackle this issue, we replace the superstrate ZnSe prime in the setup shown in Figure 1(a) by the free space $\varepsilon_{inc} = 1$, and review the performances of reflectivity $|r_p|^2$, the reflection coefficient phase $\phi_p$, and GH shifts Δ and Θ in Figure 3. Interestingly, the discrepancies of the spatial and angular GH shifts persist as well in the angle range $\theta_i \in [60°, 70°]$ where no critical angle exist and the EMT is valid according to the reflectivity. Therefore, for the GH shifts strongly dependent on the phase and magnitude of the Fresnel

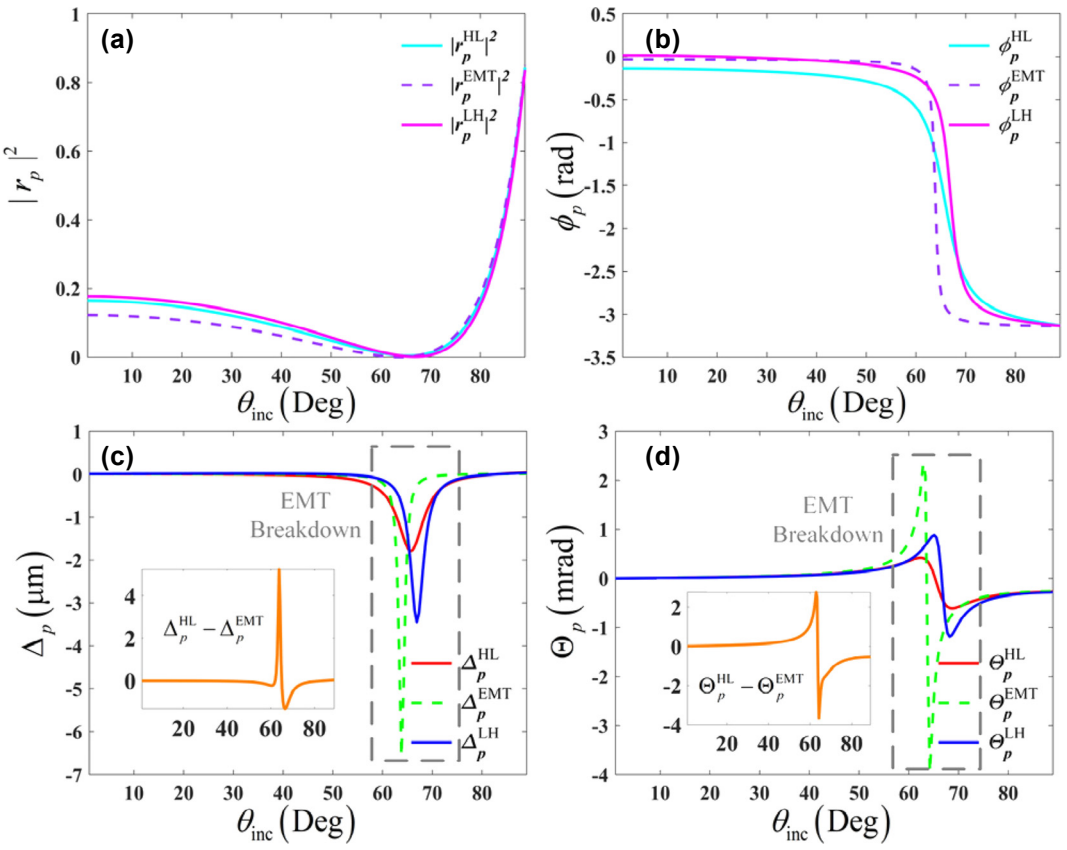


**Figure 3:** Breakdown of the EMT by the spatial (Δ) and angular (Θ) GH shifts on the all-dielectric periodic multilayered structures with different stacking orderings [*LH*] and [*HL*], in the case of $\varepsilon_{inc} = 1$. (a) Reflectivity $|r_p|^2$, (b) Fresnel reflection coefficient phase $\phi_p$, (c) spatial GH shifts (Δ), and (d) angular GH shifts (Θ).

reflection coefficient, the EMT can be disabled in any incident angles in principle. To summarize, Figures 2 and 3 illustrate that the EMT is not precise to homogenize the deep-sub-wavelength all-dielectric periodic multilayered structures when calculating the GH shifts, regardless of the existence of critical angle.

Now, we proceed to examine the breakdown of the EMT by the spatial and angular GH shifts with different polarization angle $\beta$ of incidence from Figure 4. As we can see, for the case of $\varepsilon_{inc} = 6.65$, the discrepancies in both spatial and angular GH shifts decrease with the growing polarization angle in regions far from the critical angle, whereas these discrepancies are robust against the variations of polarization angle near the critical angle. If the superstrate is free space, the errors of spatial and angular GH shifts under *p*-polarization have a pronounced peak near the incident angle $\theta_i \approx 64°$. But these errors rapidly diminish to near-zero values at larger polarization angles. These findings imply that the EMT achieves higher accuracy for larger polarization angles in the all-dielectric systems.

Figure 5 depicts the breakdown of the EMT by the spatial and angular GH shifts with different filling fraction $g$ = [0.2, 0.4, 0.6, 0.8] of the structure. The $g$ is defined as $d_1/(d_1 + d_2)$ and $d_1 + d_2 = 20$ nm is always satisfied. When a critical angle exists, the discrepancies of GH shifts will increase at first and then decrease as the filling fraction $g$ rises, reaching the maximum value, when the thicknesses of the two components are nearly identical. It means that the EMT is more exact in the all-dielectric multilayers with large differences in the thicknesses of high- and low-index layers, when its superstrate has a high relative permittivity $\varepsilon_{inc} > \varepsilon_{\perp}$. In systems without a critical angle, the discrepancies of GH shifts can be reduced via increasing the filling fraction $g$. Namely, increasing the proportion of the high-index layer in all-dielectric multilayers without the critical angle is helpful to weaken the degree of EMT breakdown.

Furthermore, we investigate the dependence of EMT breakdown induced by GH shifts on the unit-cell thickness, as shown in Figure 6. The results demonstrate that the EMT breakdown persists across a broad range of unit-cell thickness in the deep-subwavelength scale. For the case of $\varepsilon_{inc} =$

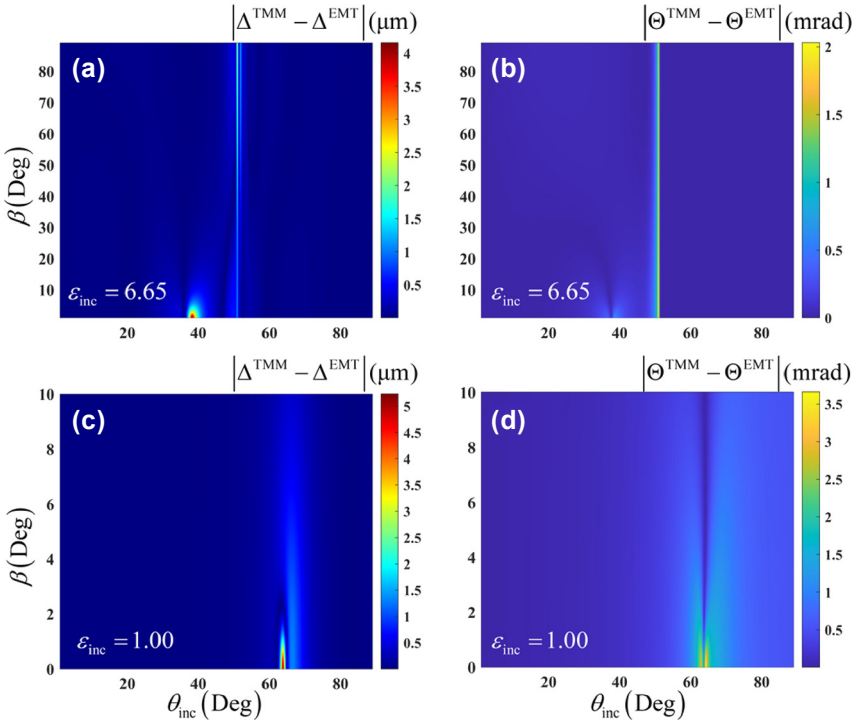


**Figure 4:** Influence of the polarization angle $\beta$ on the performance of the EMT breakdown by the spatial ($\Delta$) and angular ($\Theta$) GH shifts, in the cases of (a), (b) $\varepsilon_{inc} = 6.65$, and (c), (d) $\varepsilon_{inc} = 1$.

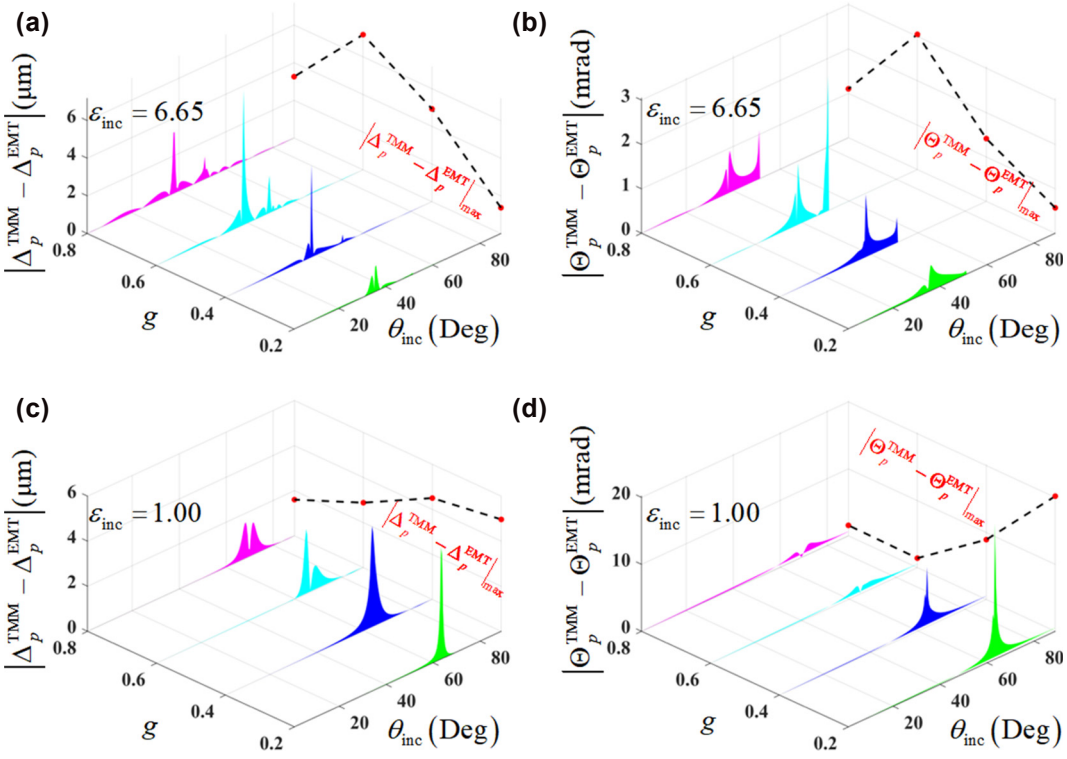


**Figure 5:** Influence of the filling fractions $g = [0.2, 0.4, 0.6, 0.8]$ of structure on the performance of the EMT breakdown by the spatial ($\Delta$) and angular ($\Theta$) GH shifts, in the cases of (a), (b) $\varepsilon_{inc} = 6.65$, and (c), (d) $\varepsilon_{inc} = 1$. The filling fraction $g = d_1/(d_1 + d_2)$, and $d_1 + d_2 = 20$ nm is always satisfied.

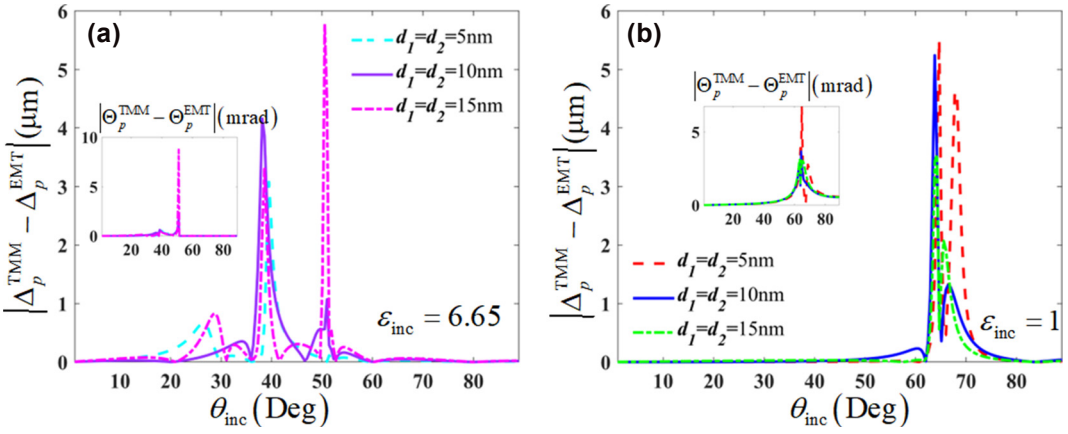


**Figure 6:** Influence of the unit-cell thickness on the performance of the EMT breakdown by the spatial (Δ) and angular (Θ) GH shifts, in the cases of (a) $\varepsilon_{inc} = 6.65$ and (b) $\varepsilon_{inc} = 1$.

6.65, the discrepancies in both spatial and angular GH shifts become larger with the growing unit-cell thickness. In contrast, when $\varepsilon_{inc} = 1$, such deviations display a decreasing trend as the unit-cell thickness increases.

In the preparation of multilayered structures, the losses of materials are inevitable. That is to say, the relative permittivities of dielectric components are generally the complex numbers with tiny imaginary parts in the experiment. In Figure 7, we examine the effects of the losses of multilayered components on the EMT. It can be seen that, the spatial and angular GH shifts still invalidate the EMT for the loss cases, and the slight losses $\mathrm{Im}(\varepsilon_{1,2}) = 0.01$ on the dielectric components have few impacts on the discrepancies in both spatial and angular GH shifts. Hence, the conclusions in our work can be generalized to the cases for the lossy multilayered structures.

According to Ref. [31], the performance of EMT breakdown rely on the periodicity number $N_{pair}$, and the severe breakdown phenomena happen only when $N_{pair} \gg 1$. Here, we perform the breakdown of the EMT for case of $N_{pair} = 1$ by the spatial and angular Θ GH shifts with the stacking ordering [*HL*] and $\varepsilon_{inc} = 1$ in Figure 8. Although on the ultrathin slab with only 30∼33 nm thickness, the spatial and angular GH shifts still contradict to the conventional EMT. Importantly, only 1 nm variation in layer thickness can make very large distinctions in GH shifts. Whereas, such ultra-sensitivity on the thickness does not exhibit via the EMT. These differences can be explained by the reflectivity $|r_p|^2$ and reflection coefficient phase $\phi_p$. The 1 nm thickness change can hardly affect the $|r_p|^2$ and $\phi_p$ in the framework of EMT, but can be demonstrated via the TMM. It indicates that the homogenization in EMT may overlook the extreme small property variations of mediums. These phenomena indicate the GH shift is a powerful tool in the detection of dielectric structure defects at the extreme nanoscale, which has been overlooked before in the framework of EMT.

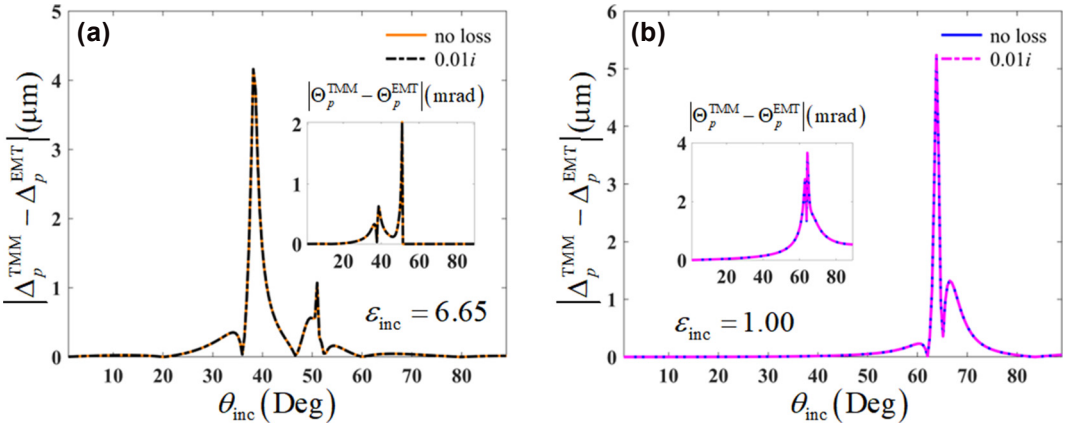


**Figure 7:** Influence of the multilayered components loss on the performance of the EMT breakdown by the spatial (Δ) and angular (Θ) GH shifts, in the cases of (a) $\varepsilon_{inc} = 6.65$ and (b) $\varepsilon_{inc} = 1$.

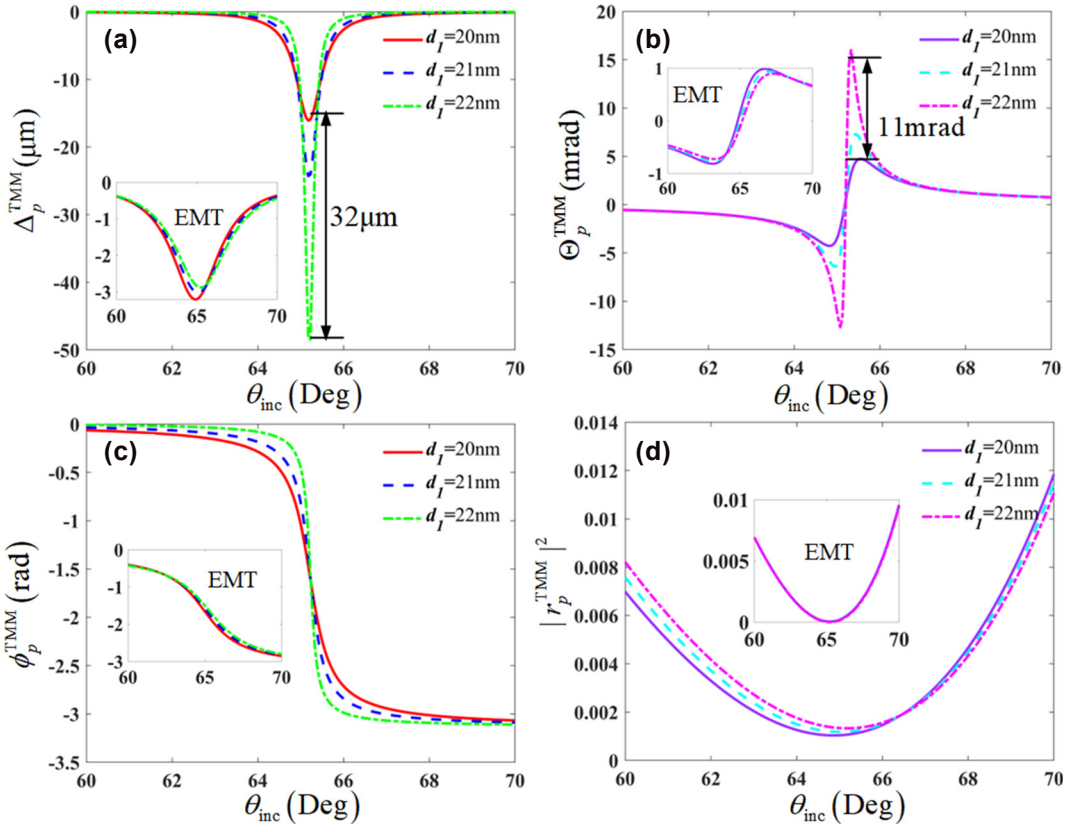


**Figure 8:** Breakdown of the EMT by the GH shifts with the stacking ordering [*HL*] in case of $\varepsilon_{inc} = 1$ and $N_{pair} = 1$, and the detection of dielectric structure defects at the extreme nanoscale. (a) spatial (Δ) GH shifts, (b) angular (Θ) GH shifts, (c) reflectivity $|r_p|^2$, and (d) Fresnel reflection coefficient phase $\phi_p$.

To experimentally validate the proposed concept, we employ the weak measurement [49] techniques in our setup. The experimental configuration begins with a Gaussian beam generated by the He–Ne laser passing through a Glan laser polarizer (GLP1) and a focusing lens (L1) before incident on the all-dielectric multilayered structures. The reflected beam then propagates through a quarter-wave plate (QWP), followed by a half-wave plate (HWP) and another Glan laser polarizer (GLP2), before being focused by a second lens (L2) onto a CCD detector for measurement. The breakdown of EMT can be experimentally demonstrated by comparing the measured GH shifts from all-dielectric multilayered structures with different stacking sequences. The weak measurement protocol enables significant amplification of the GH shift through careful selection of nearly orthogonal post-selection and preselection states. The multilayered structures, composed of alternating alumina ($Al_2O_3$) and titania ($TiO_2$) layers with designed stacking orders, are fabricated using atomic layer deposition (ALD) to ensure precise thickness control and interfacial quality.

Finally, it is worthy to note that the EMT fails to predict the reflection phase in many cases, making it ineffective for GH shifts and other phase-sensitive physical phenomena. Therefore, the careful consideration of phase-related effects is essential when evaluating the applicability of EMT. It holds significant implications for the design of novel micro-nano optoelectronic devices.

## 4 Conclusions

In conclusion, we have reported the breakdown of EMT by the spatial and angular GH shifts on the periodic deep-subwavelength multilayered dielectric structures under the general conditions. Through comparing the GH shifts calculated by the EMT and TMM, it is found that the differences between them are very large in some cases commonly discussed. The underlying mechanism behind this phenomenon is ascribed to the high sensitivity of the GH shift on the Fresnel reflection coefficient phase and magnitude. Meanwhile, the numerical results have shown that the degree of the EMT breakdown can be controlled via adjusting the polarization angle of incidence and the layer and filling fraction of the structures. Finally, we have revealed

the potential application of the GH shift on nano-meter scale thickness sensing, which may not be demonstrated within the EMT framework. This work will be helpful for improving the calculating accuracy of the electromagnetic responses and promoting the development of precise metrology devices.

**Research funding:** This work was supported by the National Natural Science Foundation of China (12374273, 12421005, 92464205), the Basic and Applied Basic Research Foundation of Guangdong Province (2023A1515030152). Hunan Provincial Major Sci-Tech Program (2023ZJ1010), Fundamental Research Funds for the Central Universities (YJSJ25020), and Innovation Fund of Xidian University.

**Author contributions:** WG: writing-original draft, investigation, data curation. YS: writing-original draft, writing-review & editing data, investigation. ZL: software. CZ: investigation. ZC: supervision, validation. YC: supervision, formal analysis. XZ: supervision, project administration, conceptualization. All authors have accepted responsibility for the entire content of this manuscript and consented to its submission to the journal, reviewed all the results and approved the final version of the manuscript.

**Conflict of interest:** Authors state no conflicts of interest.

**Data availability:** Data sharing is not applicable to this article as no datasets were generated or analyzed during the current study.

## References

[1] T. C. Choy, *Effective Medium Theory: Principles and Applications*, 2nd ed. Oxford, Oxford University Press, 2015.

[2] J. A. Kong, *Electromagnetic Wave Theory*, Cambridge, EMW Publishing, 2008.

[3] J. C. M. Garnett, "Colours in metal glasses and in metallic films," *Philos. Trans. R. Soc. Lond. A*, vol. 203, pp. 385—420, 1904.

[4] D. A. G. Bruggeman, "Calculation of various physics constants in heterogenous substances I dielectricity constants and conductivity of mixed bodies from isotropic substances," *Ann. Phys.*, vol. 416, no. 7, pp. 636—664, 1935.

[5] J. Huang, S. J. Chen, Z. Xue, W. Withayachumnankul, and C. Fumeaux, "Wideband endfire 3-D-printed dielectric antenna with designable permittivity," *IEEE Antennas Wirel. Propag. Lett.*, vol. 17, no. 11, pp. 2085—2089, 2018.

[6] J. Xin, J. Zong, J. Gao, Y. Wang, Y. Song, and X. Zhang, "Extraction and control of permittivity of hyperbolic metamaterials with optical nonlocality," *Opt. Express*, vol. 29, no. 12, pp. 18572—18586, 2021.

[7] T. Hou and H. Chen, "Criterion for photonic topological transition in two-dimensional heterostructures," *Opt. Lett.*, vol. 47, no. 20, pp. 5433—5436, 2022.

[8] N. Wang, R.-Y. Zhang, C. T. Chen, and G. P. Wang, "Effective medium theory for a photonic pseudospin -1/2 system," *Phys. Rev. B*, vol. 102, no. 9, p. 094312, 2020.

[9] F. Liu, P. Peng, Q. Du, and M. Ke, "Effective medium theory for photonic crystals with quadrupole resonances," *Opt. Lett.*, vol. 46, no. 18, pp. 4597—4600, 2021.

[10] A. Vakil and N. Engheta, "Transformation optics using graphene," *Science*, vol. 332, no. 6035, pp. 1291—1294, 2011.

[11] B. Rahmani, A. Bagheri, A. Khavasi, and K. Mehrany, "Effective medium theory for graphene-covered metallic gratings," *J. Opt.*, vol. 18, no. 10, p. 105005, 2016.

[12] I. O. Thomas and G. P. Sriastava, "Extension of the modified effective medium approach to nanocomposites with anisotropic thermal conductivities," *Phys. Rev. B*, vol. 98, no. 9, p. 094201, 2018.

[13] F. Xu, R.-C. Tyan, P.-C. Sun, Y. Fainman, C.-C. Cheng, and A. Scherer, "Fabrication, modeling, and character- ization of form-birefringent nanostructures," *Opt. Lett.*, vol. 20, no. 24, pp. 2457—2459, 1995.

[14] M. Segev, Y. Silberberg, and D. N. Christodoulides, "Anderson localization of light," *Nat. Photonics*, vol. 7, no. 3, pp. 197—204, 2013.

[15] V. M. Shalaev, *et al*., "Negative index of refraction in optical metamaterials," *Opt. Lett.*, vol. 30, no. 24, pp. 3356—3358, 2005.

[16] X. Zhang, M. Davanço, Y. Urzhumov, G. Shvets, and S. R. Forrest, "From scattering parameters to Snell's Law: A subwavelength near-infrared negative-index metamaterial," *Phys. Rev. Lett.*, vol. 101, no. 26, p. 267401, 2008.

[17] V. M. Shalaev, "Optical negative-index metamaterials," *Nat. Photonics*, vol. 1, no. 1, pp. 41—48, 2007.

[18] R. J. Pollard, *et al*., "Optical nonlocalities and additional waves in epsilon-near-zero metamaterials," *Phys. Rev. Lett.*, vol. 102, no. 12, p. 127405, 2009.

[19] R. Maas, J. Parsons, N. Engheta, and A. Polman, "Experimental realization of an epsilon-near-zero metamaterial at visible wavelengths," *Nat. Photonics*, vol. 7, no. 11, pp. 907—912, 2013.

[20] S. Sun, Q. He, S. Xiao, Q. Xu, X. Li, and L. Zhou, "Gradient-index meta-surfaces as a bridge linking propagating waves and surface waves," *Nat. Mater.*, vol. 11, no. 5, pp. 426—431, 2012.

[21] A. V. Kildishev, A. Boltasseva, and V. M. Shalaev, "Planar photonics with metasurfaces," *Science*, vol. 339, no. 6125, p. 1232009, 2013.

[22] X. Yin, Z. Ye, J. Rho, Y. Wang, and X. Zhang, "Photonic spin Hall effect at metasurfaces," *Science*, vol. 339, no. 6126, pp. 1405—1407, 2013.

[23] J. Valentine, J. Li, T. Zentgraf, G. Bartal, and X. Zhang, "An optical cloak made of dielectrics," *Nat. Mater.*, vol. 8, no. 7, pp. 568—571, 2009.

[24] T. Cai, *et al*., "Experimental realization of a superdispersion-enabled ultrabroadband terahertz cloak," *Adv. Mater.*, vol. 34, no. 38, p. 2205053, 2022.

[25] J. B. Pendry, "Negative refraction makes a perfect lens," *Phys. Rev. Lett.*, vol. 85, no. 18, p. 3966, 2000.

[26] X. Zhang and Z. Liu, "Superlenses to overcome the diffraction limit," *Nat. Mater.*, vol. 7, no. 6, pp. 435—441, 2008.

[27] N. Fang, H. Lee, C. Sun, and X. Zhang, "Sub-diffraction-limited optical imaging with a silver superlens," *Science*, vol. 308, no. 5721, pp. 534—537, 2005.

[28] F. Wang and Y. R. Shen, "General properties of local plasmons in metal nanostructures," *Phys. Rev. Lett.*, vol. 97, no. 20, p. 206806, 2006.

[29] O. Kidwai, S. V. Zhukovsky, and J. E. Sipe, "Effective-medium approach to planar multilayer hyperbolic metamaterials: Strengths and limitations," *Phys. Rev. A*, vol. 85, no. 5, p. 053842, 2012.

[30] M. Mahmoodi, S. H. Tavassoli, O. Takayama, J. Sukham, R. Malureanu, and A. V. Lavrinenko, "Existence conditions of high-k modes in finite hyperbolic metamaterials," *Laser Photonics Rev.*, vol. 13, no. 3, p. 1800253, 2019.
[31] H. H. Sheinfux, I. Kaminer, Y. Plotnik, G. Bartal, and M. Segev, "Subwavelength multilayer dielectrics: Ultrasensitive transmission and breakdown of effective-medium theory," *Phys. Rev. Lett.*, vol. 113, no. 24, p. 243901, 2014.
[32] S. V. Zhukovsky, *et al*., "Experimental demonstration of effective medium approximation breakdown in deeply subwavelength all-dielectric multilayers," *Phys. Rev. Lett.*, vol. 115, no. 17, p. 177402, 2015.
[33] H. H. Sheinfux, I. Kaminer, A. Z. Genack, and M. Segev, "Interplay between evanescence and disorder in deep subwavelength photonic structures," *Nat. Commun.*, vol. 7, no. 1, p. 12927, 2016.
[34] H. H. Sheinfux, Y. Lumer, G. Ankonina, A. Z. Genack, G. Bartal, and M. Segev, "Observation of Anderson localization in disordered nanophotonic structures," *Science*, vol. 356, no. 6341, pp. 953—956, 2017.
[35] S. Yuan, *et al*., "Breakdown of effective-medium theory by a photonic spin Hall effect," *Sci. China Phys. Mech. Astron.*, vol. 66, no. 11, p. 114212, 2023.
[36] F. Goos and H. Hachen, "Ein neuer und fundamentaler Versuch zur Totalreflexion," *Ann. Phys.*, vol. 1, nos. 7—8, pp. 333—346, 1947.
[37] M. Luo and F. Wu, "Refractive-index sensing based on large negative Goos-Hänchen shifts of a wavy dielectric grating," *Phys. Rev. Appl.*, vol. 22, no. 1, p. 01450, 2024.
[38] Y. Xi, L. Wu, and L. K. Ang, "Surface exciton polariton enhanced Goos-Hänchen and Imbert-Fedorov shifts and their applications in refractive index sensing," *Opt. Express*, vol. 32, no. 7, pp. 11171—11181, 2024.
[39] H. Pourhassan, E. Safari, M. R. Tohidkia, and A. Aghanejad, "Oxygen sensing of hemoglobin states by Goos-Hänchen effect," *Opt. Laser Tech.*, vol. 148, p. 107756, 2022.
[40] C. Xu, J. Xu, G. Song, C. Zhu, Y. Yang, and G. S. Agarwal, "Enhanced displacements in reflected beams at hyperbolic metamaterials," *Opt. Express*, vol. 24, no. 19, pp. 21767—21776, 2016.
[41] E. N. Afshar and A. Namdar, "Temperature dependence of the Goos-Hänchen shift in the nonlinear metal-dielectric nanocomposites," *Opt. Quant. Electron.*, vol. 51, no. 8, p. 258, 2019.
[42] M. Zoghi, "Reflection shifts in a graphene-coated dielectric—metal composite of non-spherical particles," *Opt. Commun.*, vol. 451, pp. 160—167, 2019.
[43] P. Yeh, *Optical Wave in Layered Media*, New York, Wiley, 1988.
[44] Z. Xiao, H. Luo, and S. Wen, "Goos-Hanchen and Imbert-Fedorov shifts of vortex beams at air-left-handed-material interfaces," *Phys. Rev. A*, vol. 85, no. 5, p. 053822, 2012.
[45] J. R. Devore, "Refractive indices of rutile and sphalerite," *J. Opt. Soc. Am. A*, vol. 41, no. 6, pp. 416—419, 1951.
[46] I. H. Malitson, F. V. Murphy, and W. S. Rodney, "Refractive index of synthetic sapphire," *J. Opt. Soc. Am. A*, vol. 48, no. 1, pp. 72—73, 1958.
[47] D. T. F. Marple, "Refractive index of ZnSe, ZnTe, and CdTe," *J. Appl. Phys.*, vol. 35, no. 3, pp. 539—542, 1964.
[48] T. Bååk, "Silicon oxynitride: A material for GRIN optics," *Appl. Opt.*, vol. 21, no. 6, pp. 1069—1072, 1982.
[49] S. Chen, C. Mi, L. Cai, M. Liu, H. Luo, and S. Wen, "Observation of the Goos-Hänchen shift in graphene via weak measurements," *Appl. Phys. Lett.*, vol. 110, no. 3, p. 031105, 2017.